Electronic Supplementary Material (ESI) for Catalysis Science & Technology.
This journal is © The Royal Society of Chemistry 2018

Supplementary Material

Dimethyl ether carbonylation to methyl acetate over highly crystalline zeolite-seed derived ferrierite

Jihyeon Kim, Hyungwon Ham, Hyun Seung Jung, Yang Wang, Yingluo He, Noritatsu Tsubaki, Sung June Cho*, Gui Young Han, Jong Wook Bae**

Figure S5. FT-IR spectra of the adsorbed DME in the range of 1500 – 2000 cm^{-1} at different temperatures on the fresh seed-derived FER zeolites synthesized from various zeolite seeds

Figure S6. FT-IR spectra of the adsorbed DME in the range of 3100 – 3900 cm^{-1} at different temperatures on the fresh seed-derived FER zeolites synthesized from various zeolite seeds

Figure S7. Correlations of methanol conversions to DME with the amount of weak acid sites (measured by NH_3-TPD) on the solid-acid heterogeneous catalysts (mainly, Al_2O_3 and zeolites), where too larger amounts of acidic sites can also generate some coke precursors by keeping the dehydration activity constant

Figure S8. Rietveld refinement plot of four different seed-derived FER zeolites such as (A) FER, (B) FER@FER, (C) MOR@FER, (D) ZSM-5@FER and (E) USY@FER

Figure S9. NMR spectra of the fresh seed-derived FER zeolites with ^{27}Al MAS NMR spectra, ^{29}Si MAS NMR spectra and deconvoluted area (%) of the Al-O-Si structures

Figure S10. Equilibrium conversions of DME carbonylation to methyl acetate at the fixed pressure of 1.0 MPa with respect to reaction temperatures (100 – 400 ^{o}C) and CO/DME molar ratios (1 – 30)

Figure S11. Variations of FT-IR spectra of the adsorbed methyl intermediates appeared at the bands of 2968 and 2949 cm^{-1} on the fresh FER and FER@FER through a successive adsorption experiment of DME followed by CO reactant at a fixed temperature of 220 ^{o}C

Scheme S1. Proposed reaction mechanisms on the highly crystalline FER@FER

Calculations of the mass- and heat-transfer limitations [S1] for the DME carbonylation reaction to methyl acetate on the most active FER@FER were verified at the reaction conditions of T = 220 °C, P = 1.0 MPa, and space velocity (SV) of 2000 L/($kg_{cat}\cdot h$) using a mixed gas reactant of DME/CO/N_2(mol%) = 5/45/50.

(1) Mears Criterion for External Diffusion (Fogler, p841; Mears, 1971)

If $\frac{-r_A' \rho_b R n}{k_c C_{Ab}} < 0.15$, then external mass transfer is not limited

$-r_A'$ = observed reaction rate, kmol-C_3/$kg_{cat}\cdot s$

n = reaction order

R = catalyst particle radius, m

ρ_b = bulk density of catalyst bed, kg/m^3 = $\rho_c(1-\phi)$ (ϕ= porosity or void fraction of packed bed)

ρ_c = solid catalyst density, kg/m^3

C_{Ab} = bulk gas concentration of propane, kmol/m^3

k_c = mass transfer coefficient, m/s

$\frac{-r_A' \rho_b R n}{k_c C_{Ab}}$ = [1.60×10^{-7} kmol-C_3/$kg_{cat}\cdot s$] × [47.3 kg/m^3] × [3×10^{-5} m] × [1] / ([11.20 m/s] × [0.0032 kmol/m^3]) **= $6.3 \times 10^{-11} < 0.15$ → External diffusion is not limited.**

(2) Weisz-Prater Criterion for Internal Diffusion (Fogler, p839)

If $C_{WP} = \frac{-r'_{A(obs)} \rho_c R^2}{D_e C_{As}} < 1$, then internal mass transfer is not limited

$-r'_{A(obs)}$ = observed reaction rate, kmol-C_3/$kg_{cat}\cdot s$

R = catalyst particle radius, m

ρ_c = solid catalyst density, kg/m^3; [$\rho_{c,FER}$ = 1493 kg/m^3]

D_e = effective gas-phase diffusivity, m^2/s **[Fogler, p815]**

$$= \frac{D_{AB}\phi_p\sigma_c}{\tau}$$ where

D_{AB} = gas-phase diffusivity m^2/s; ϕ_p = pellet porosity; σ_c =constriction factor; τ =tortuosity.

C_{As} = gas concentration of propane at the catalyst surface, kmol-C_3/m^3

$$C_{WP} = \frac{-r'_{A(obs)}\,\rho_c R^2}{D_e C_{As}}$$ = [1.60 × 10^{-7} kmol-C_3/kg$_{cat}$·s] × [1493 kg/m^3] × [3 × 10^{-5} m]^2 / ([2.93 × 10^{-6} m^2/s] × [9.67 × 10^{-6} kmol-C_3/m^3]) = **7.6 × 10^{-7} < 1 → Internal diffusion is not limited.**

(3) Mears Criterion for External (Interphase) Heat Transfer (Fogler, p842)

If $\left|\frac{-\Delta H_r(-r_A')\rho_b RE}{h_t T_b^2 R_g}\right| < 0.15$, then external heat transfer is not limited

ΔH_r = Heat of reaction, kJ/mol

$-r_A'$ = observed reaction rate, kmol-C_3/kg$_{cat}$·s

ρ_b = bulk density of catalyst bed, kg/m^3 = $\rho_c(1-\phi)$ (ϕ= porosity or void fraction of packed bed)

R = catalyst particle radius, m

E = activation energy of the reaction, kJ/kmol

n = reaction order

h_t = heat transfer coefficient, kJ/m^2·K·s

T_b = bulk gas temperature, K

R_g = gas constant, 8.314 x 10^{-3} kJ/mol·K

$\left|\frac{-\Delta H_r(-r_A')\rho_b RE}{h_t T_b^2 R_g}\right|$ = ([118.7 kJ/mol] × [1.60 × 10^{-7} kmol-C_3/kg$_{cat}$·s] × [47.3 kg/m^3] × [3 × 10^{-5} m] × [95 kJ/mol]) / ([40.92 kJ/m^2.K.s] × [493.15 K]^2 × [8.314 × 10^{-3} kJ/mol.K]) = **3.1 × 10^{-13} < 0.15 → External heat transfer is not limited.**

(4) Mears Criterion for Combined Interphase and Intraparticle Heat and Mass Transport (Mears, 1971)

If $\frac{-r'_A R^2}{C_{Ab} D_e} < \frac{1+0.33\gamma\chi}{|n-\gamma_b\beta_b|(1+0.33n\omega)}$, interphase and intraparticle heat and mass transport are not limited When

$$\gamma = \frac{E}{R_g T_s};\quad \gamma_b = \frac{E}{R_g T_b};\quad \beta_b = \frac{(-\Delta H_r)D_e C_{Ab}}{\lambda T_b};\quad \chi = \frac{(-\Delta H_r)-r'_A R}{h_t T_b};\quad \omega = \frac{-r'_A R}{k_c C_{Ab}}$$

γ = Arrhenius number; β_b = heat generation function

λ = catalyst thermal conductivity, W/m·K

χ = Damköhler number for interphase heat transport

ω = Damköhler number for interphase mass transport

$-r_A'$ = observed reaction rate, kmol-C_3/kg_{cat}·s

R = catalyst particle radius, m

C_{Ab} = bulk gas concentration of propane, kmol/m^3

D_e = effective gas-phase diffusivity, m^2/s

$\frac{-r'_A R^2}{C_{Ab} D_e}$ = ([1.60 × 10^{-7} kmol-C_3/kg_{cat}·s] × [3 × 10^{-5}m]^2) / ([0.0032 kmol/m^3] × [2.9 × 10^{-6} m^2/s]) = **1.5 × 10^{-12} < 3 → Interphase and Intraparticle Heat and Mass Transport are not limited.**

[S1] S.T. Oyama, X. Zhang, J. Lu, Y. Gu, T. Fujitani, J. Catal. 257 (2008) 1-4.

Table S1. DME conversion and product distribution on the seed-derived FER zeolites synthesized by using various zeolite seeds[a] and commercial FER zeolite (CFER)

Notation	Conversion of DME (%)	Deactivation rate (%/h)[b]	Selectivity (C-mol%)			Yield of MA (%)
			MA	methanol	HC[c]	
FER	55.4	0.12	95.4	2.5	2.1	52.9
FER@FER	71.5	0.07	99.2	0.5	0.3	70.9
MOR@FER	42.5	0.23	95.2	2.8	2.0	40.5
ZSM-5@FER	30.7	0.14	89.7	4.7	5.6	27.5
USY@FER	33.8	0.13	94.2	3.9	1.9	31.8
CFER (@200 °C)[d]	10.9	-	86.8	11.1	2.1	9.5
CFER (@220 °C)[d]	14.8	-	80.5	15.3	4.2	11.9
CFER (@240 °C)[d]	15.5	-	91.4	6.3	2.3	14.2

[a] The conversions and selectivities were presented using the averaged values at the reaction duration of 80 -100 h.

[b] The deactivation rate (%/h) of the various zeolites coated with ferrierite was calculated by using the equation of [(maximum conversion of DME – conversion of DME at 100 h)/(reaction duration), which was further normalized using total Bronsted acid sites.

[c] HC represents the formed hydrocarbons, mainly CH_4,

[d] The CFER represents the commercial FER (Si/Al ratio = 10.4) zeolites, and the activity was measured at the reaction conditions of T = 220 - 240 °C, P = 1.0 MPa, and space velocity (SV) of 2000 L/(kg_{cat}·h) using a mixed gas reactant of DME/CO/N_2(mol%) = 5/45/50.

Table S2. Crystallographic parameters for the seed-derived FER zeolites analyzed by Rietveld refinement analysis from XRD data[a]

sample	a (Å)	b (Å)	c (Å)	V (Å^3)	R_p(%)	R_{wp}(%)
FER	18.864(3)	14.1017(17)	7.4511(9)	1982.1(4)	6.58	8.48
FER@FER	18.875(3)	14.1068(17)	7.4516(8)	1984.1(4)	6.72	8.79
MOR@FER	18.872(3)	14.1020(2)	7.4510(10)	1982.9(5)	6.35	8.27
ZSM-5@FER	18.856(4)	14.0990(2)	7.4516(10)	1981.0(5)	5.72	7.57
USY@FER	18.857(3)	14.1033(16)	7.4535(8)	1982.2(4)	6.09	7.83

[a] The space group for FER zeolite is Immm

Table S3. Bond valences for the seed-derived FER zeolites analyzed by Rietveld refinement analysis from XRD data[a]

sample	Bond valence			
	T1 (16)	T2 (8)	T3 (8)	T4 (4)
FER	4.24(15)	3.91(18)	4.0(2)	4.3(3)
FER@FER	4.46(17)	3.76(19)	4.2(2)	4.2(3)
MOR@FER	4.31(17)	3.86(19)	3.9(2)	4.3(3)
ZSM-5@FER	4.27(16)	3.81(18)	4.2(2)	4.8(3)
USY@FER	4.27(14)	3.98(17)	4.1(19)	4.4(3)
	Lattice energy per T atom (eV)			
	-125.17159	-125.2895731	-125.2865822	-125.4194282

[a] The ρ and b are 1.624 and 0.389, respectively

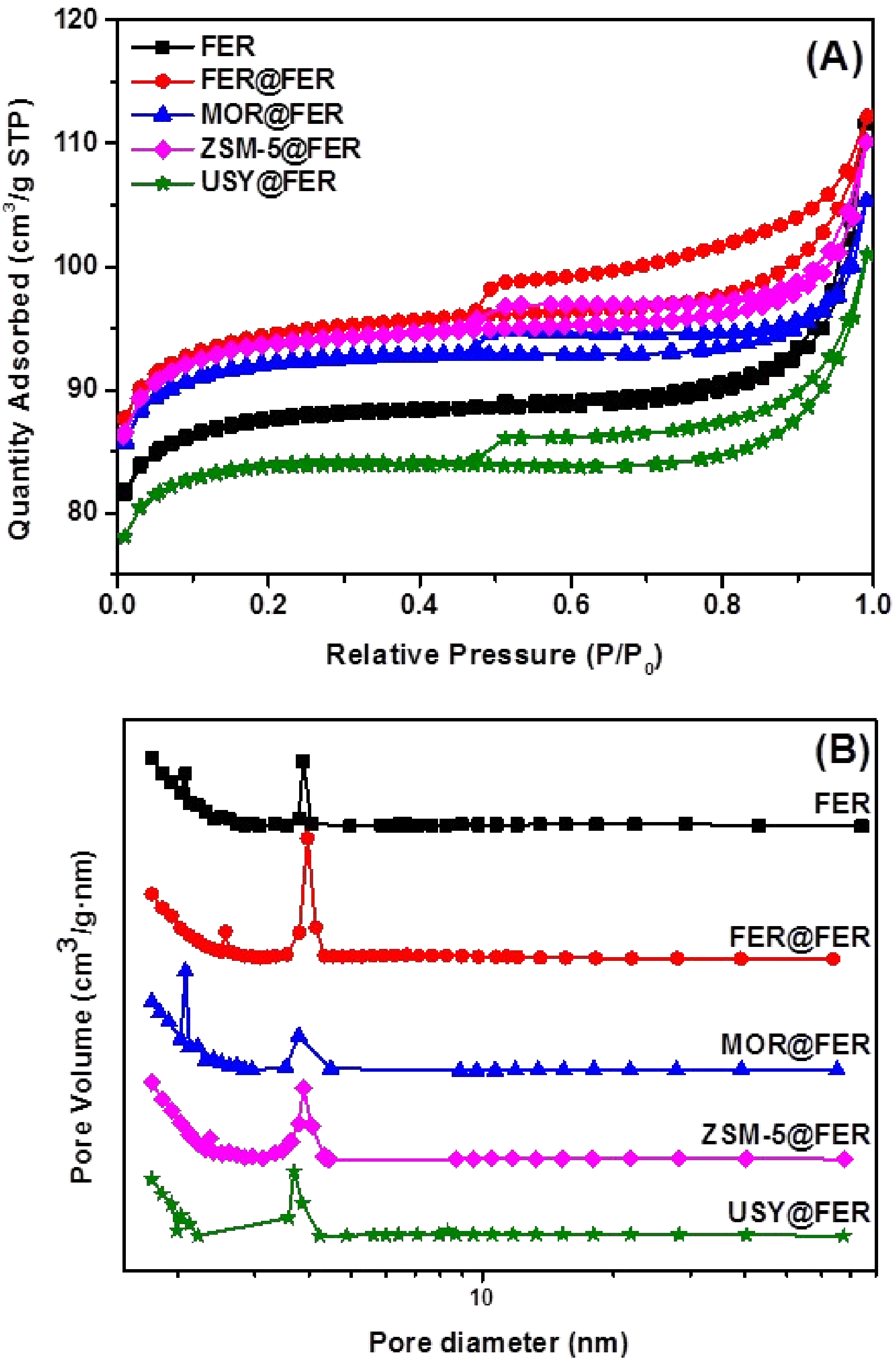

Figure S1. (A) N_2 adsorption-desorption isotherms and (B) pore size distribution of the fresh seed-derived FER zeolites prepared by using various zeolite seeds

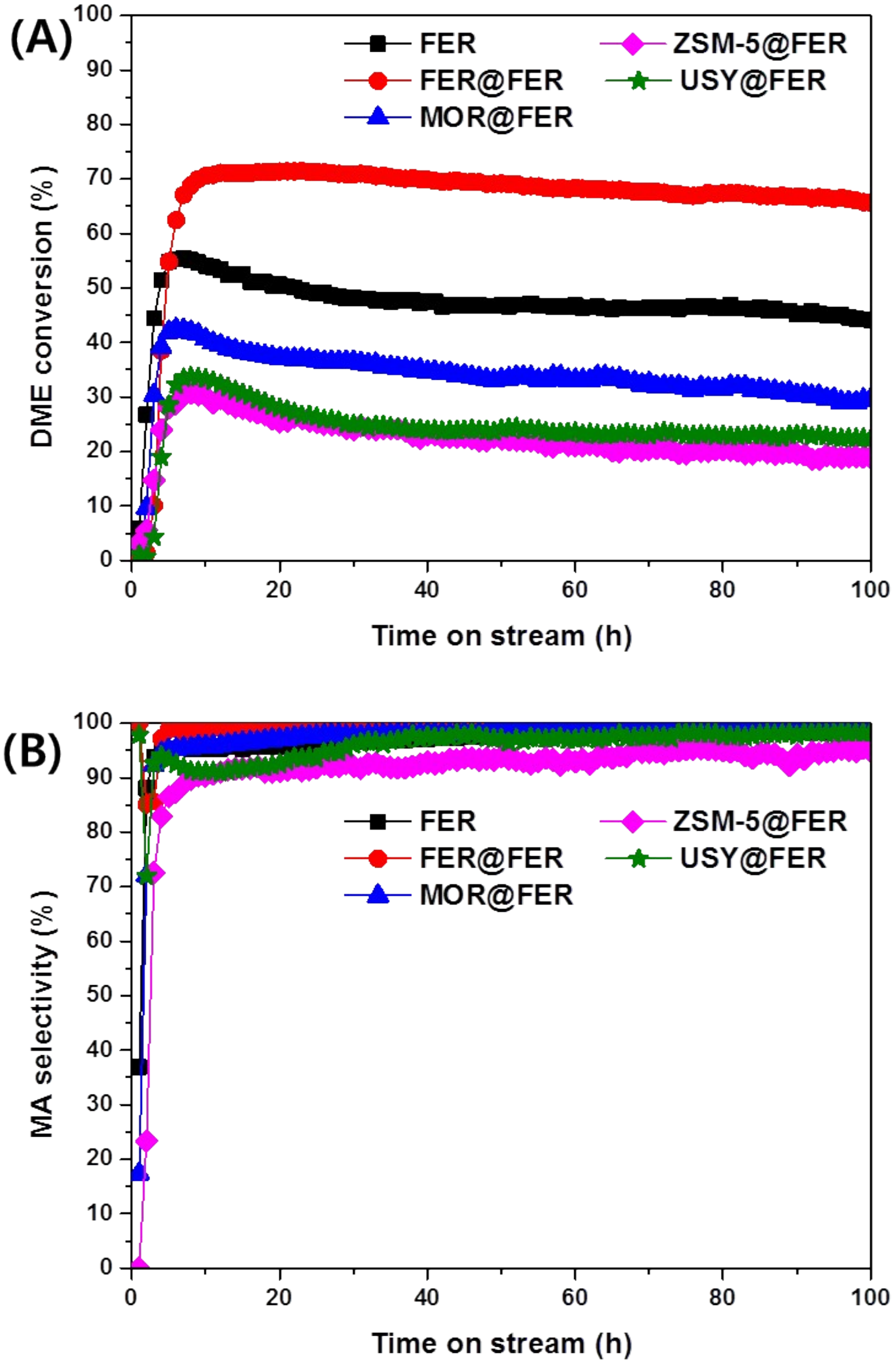

Figure S2. (A) DME conversion and (B) MA selectivity with time on stream on the seed-derived FER zeolites prepared by using various zeolite seeds

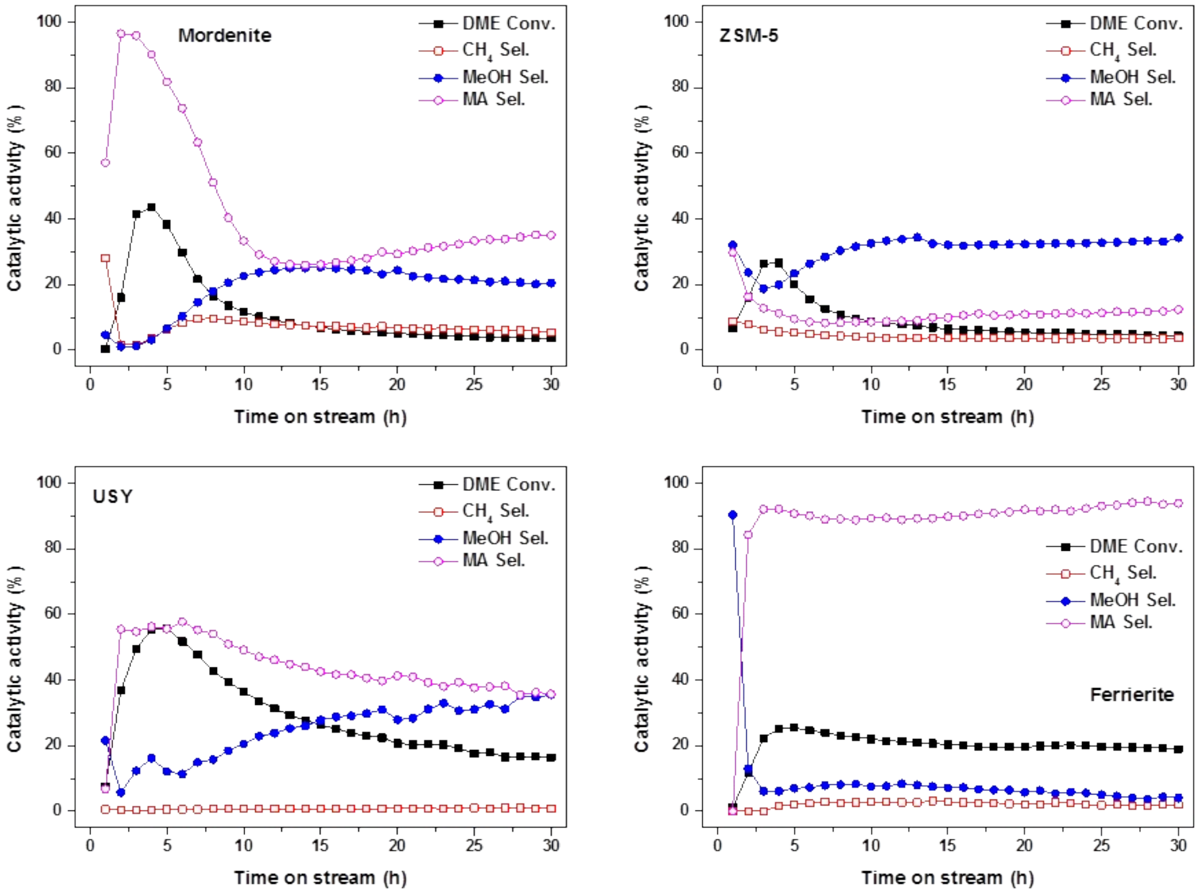

Figure S3. DME conversion and product distribution with time on stream (h) on the various pristine zeolites out at T = 220 °C, P = 1.0 MPa, and space velocity (SV) of 2000 L/(kg$_{cat}$·h) using a mixed gas reactant of DME/CO/N_2(mol%) = 5/45/50

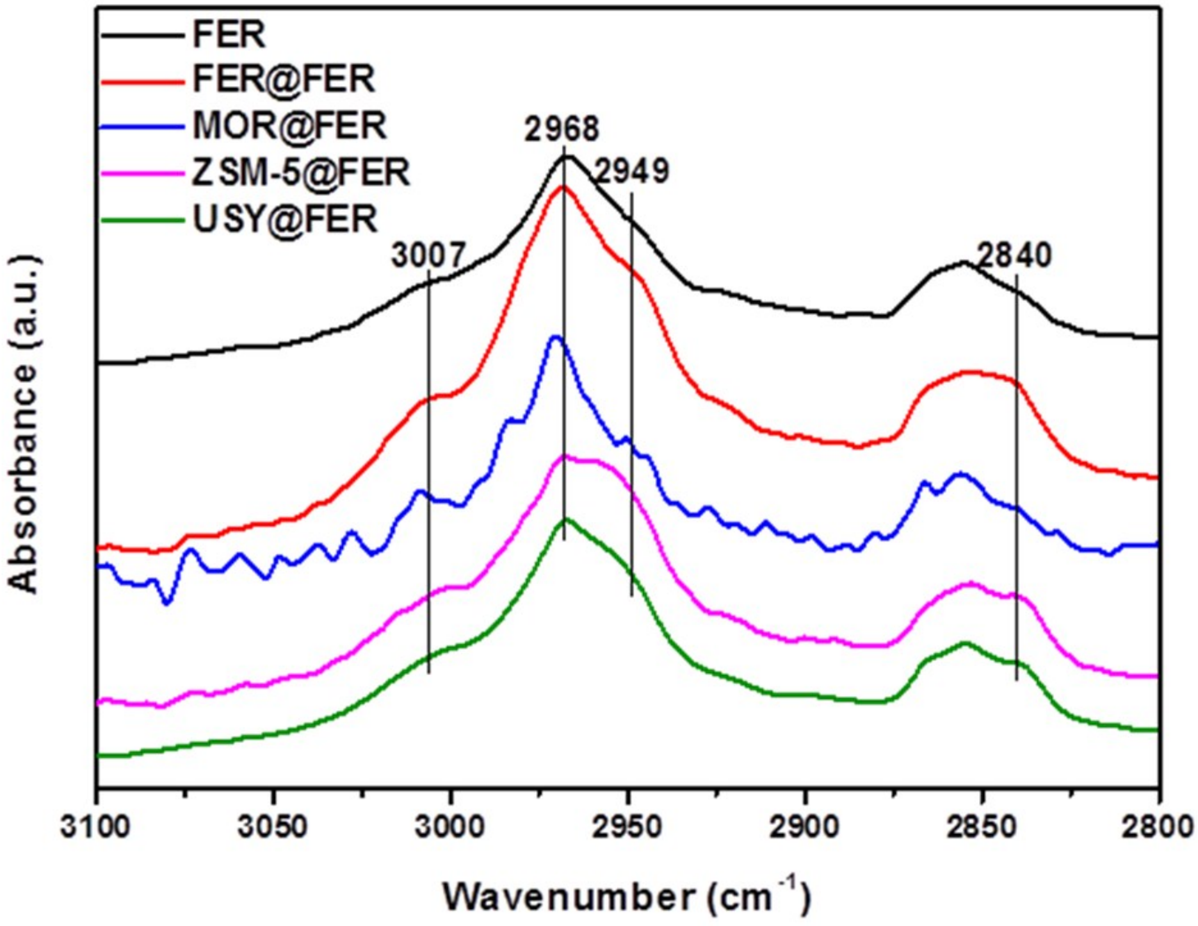

Figure S4. FT-IR spectra of the adsorbed DME at 200 ^{o}C on the fresh seed-derived FER zeolites synthesized from various zeolite seeds

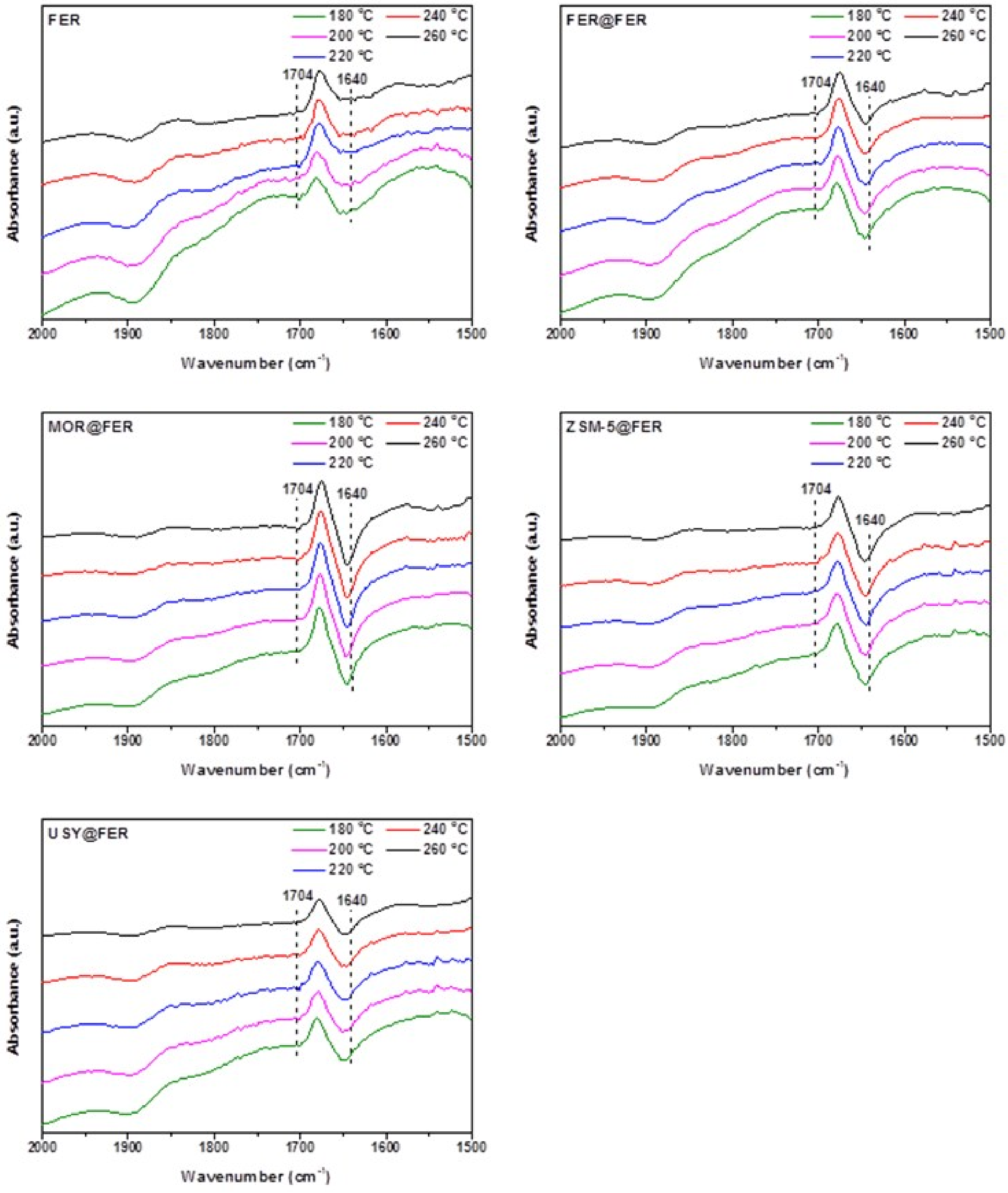

Figure S5. FT-IR spectra of the adsorbed DME in the range of 1500 – 2000 cm^{-1} at different temperatures on the fresh seed-derived FER zeolites synthesized from various zeolite seeds

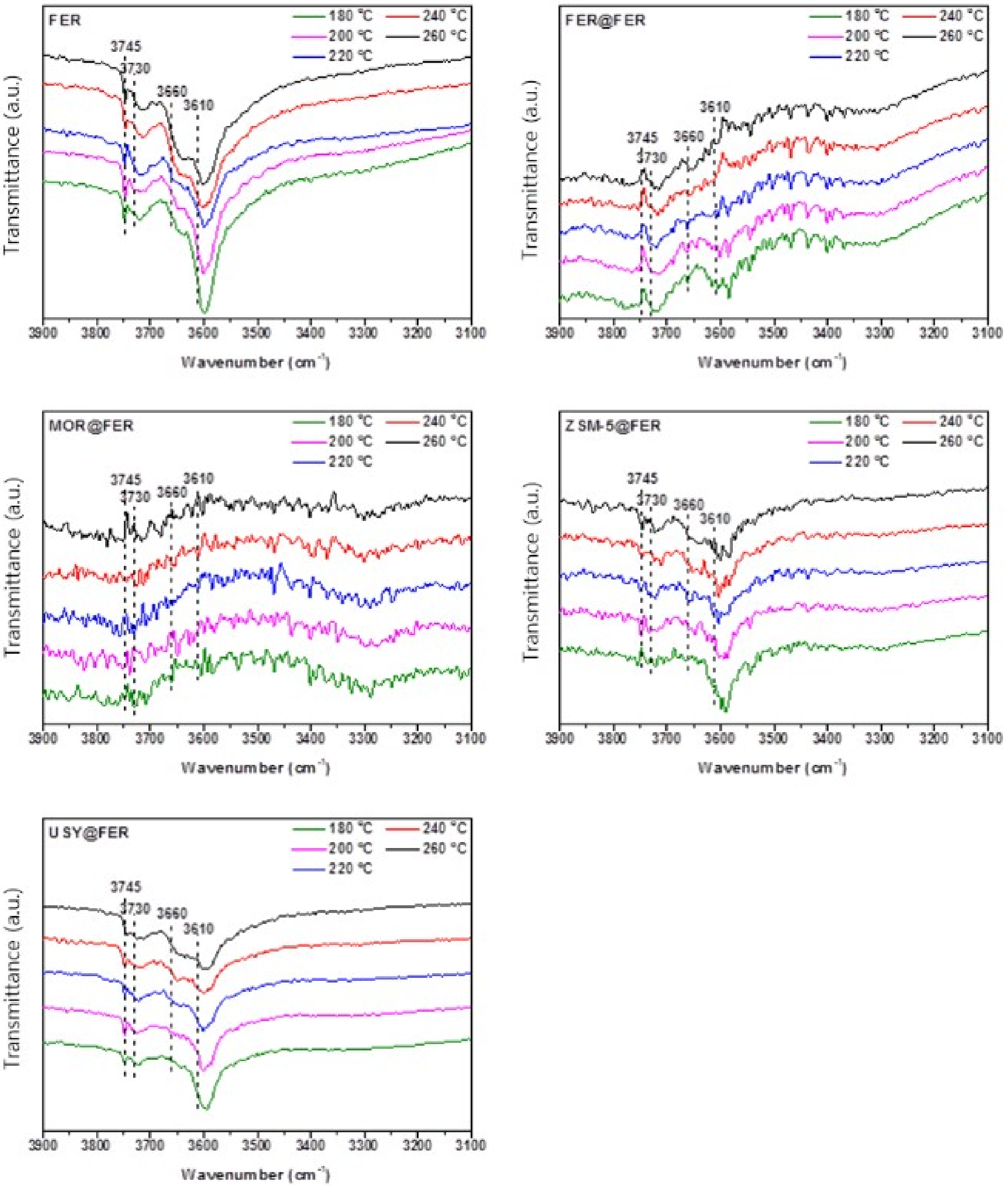

Figure S6. FT-IR spectra of the adsorbed DME in the range of 3100 – 3900 cm^{-1} at different temperatures on the fresh seed-derived FER zeolites synthesized from various zeolite seeds

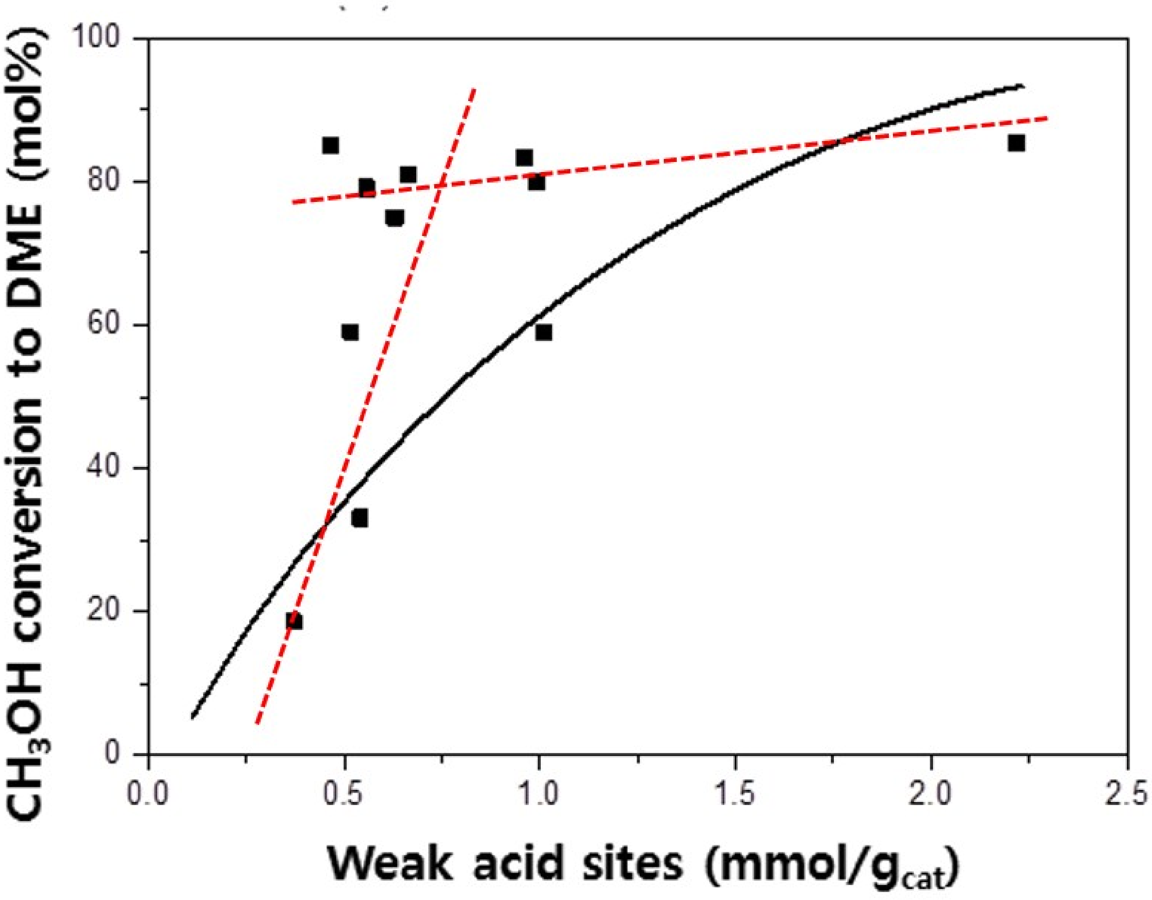

Figure S7. Correlations of methanol conversions to DME with the amount of weak acid sites (measured by NH_3-TPD) on the solid-acid heterogeneous catalysts (mainly, Al_2O_3 and zeolites), where too larger amounts of acidic sites can also generate some coke precursors by keeping the dehydration activity constant

(A) FER

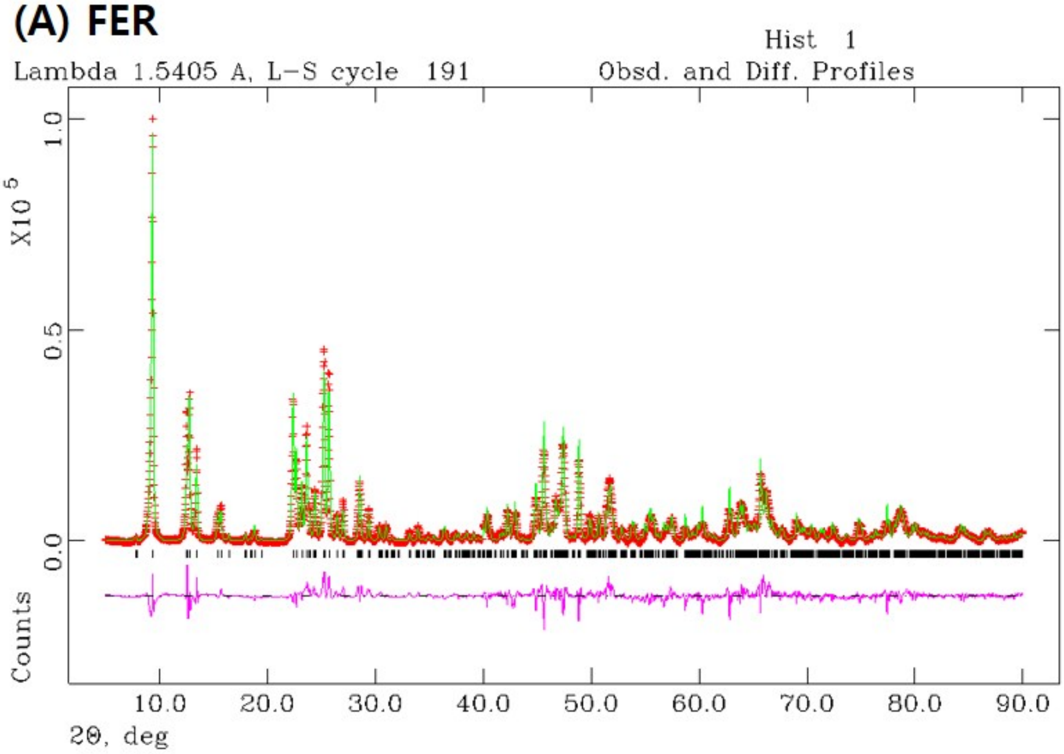

Scaling: 40.0(5.0X)

(B) FER@FER

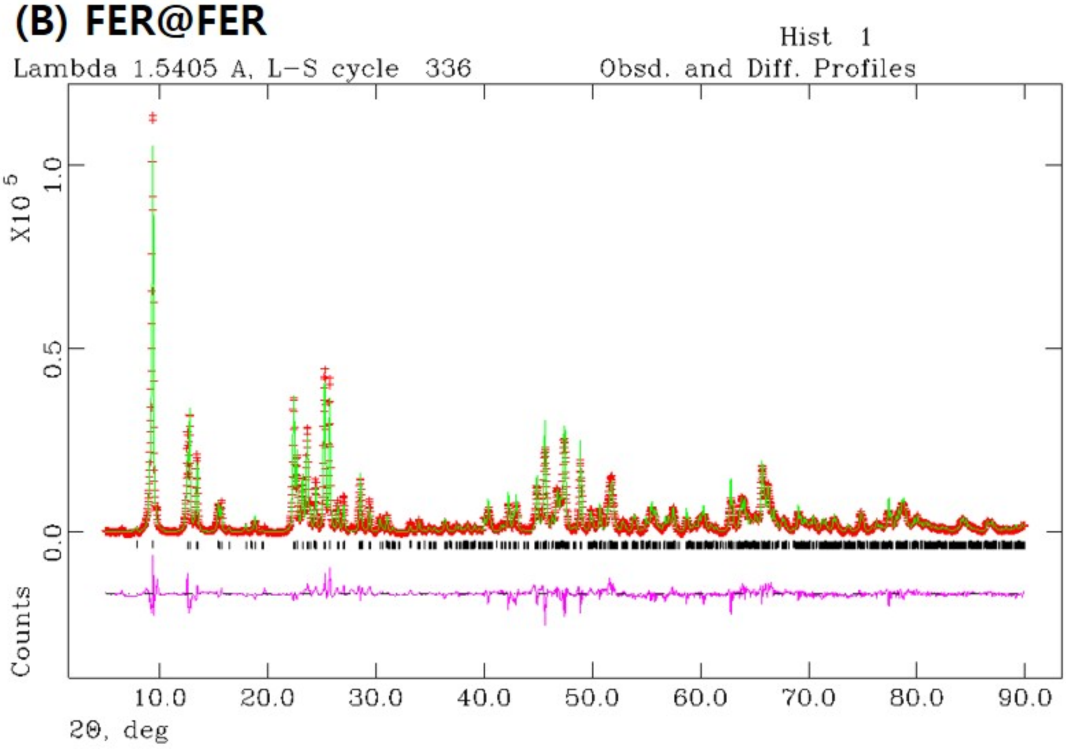

Scaling: 40.0(5.0X)

Figure S8. Rietveld refinement plot of four different seed-derived FER zeolites such as (A) FER, (B) FER@FER, (C) MOR@FER, (D) ZSM-5@FER and (E) USY@FER

(C) MOR@FER

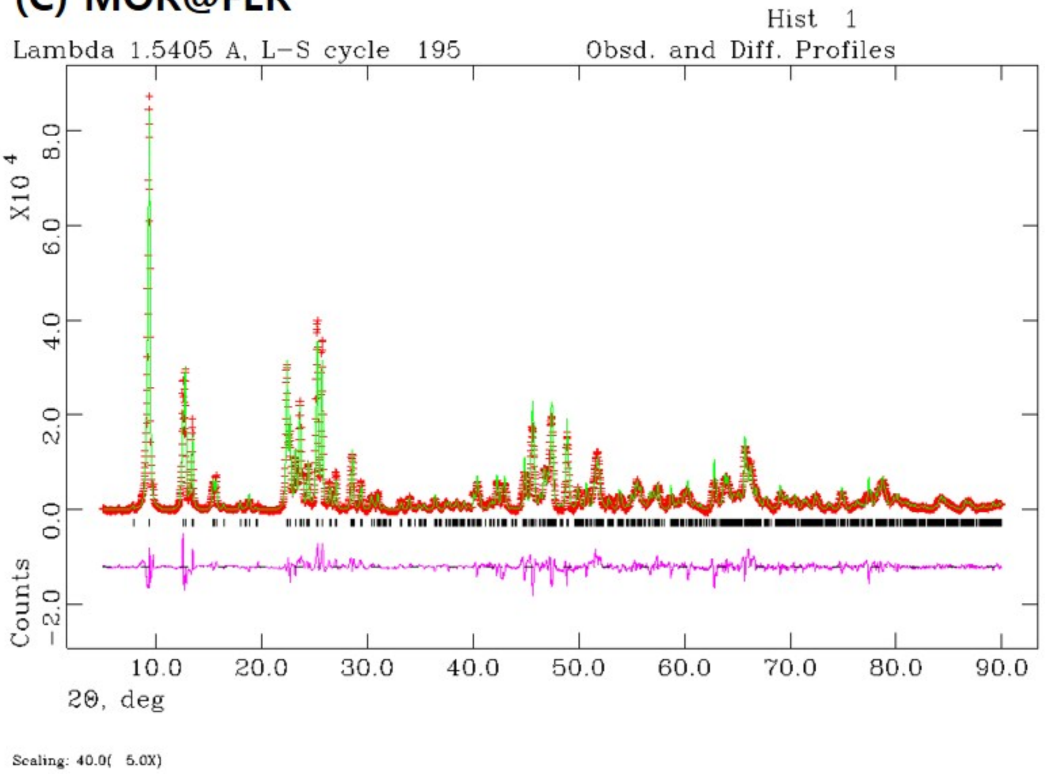

(D) ZSM-5@FER

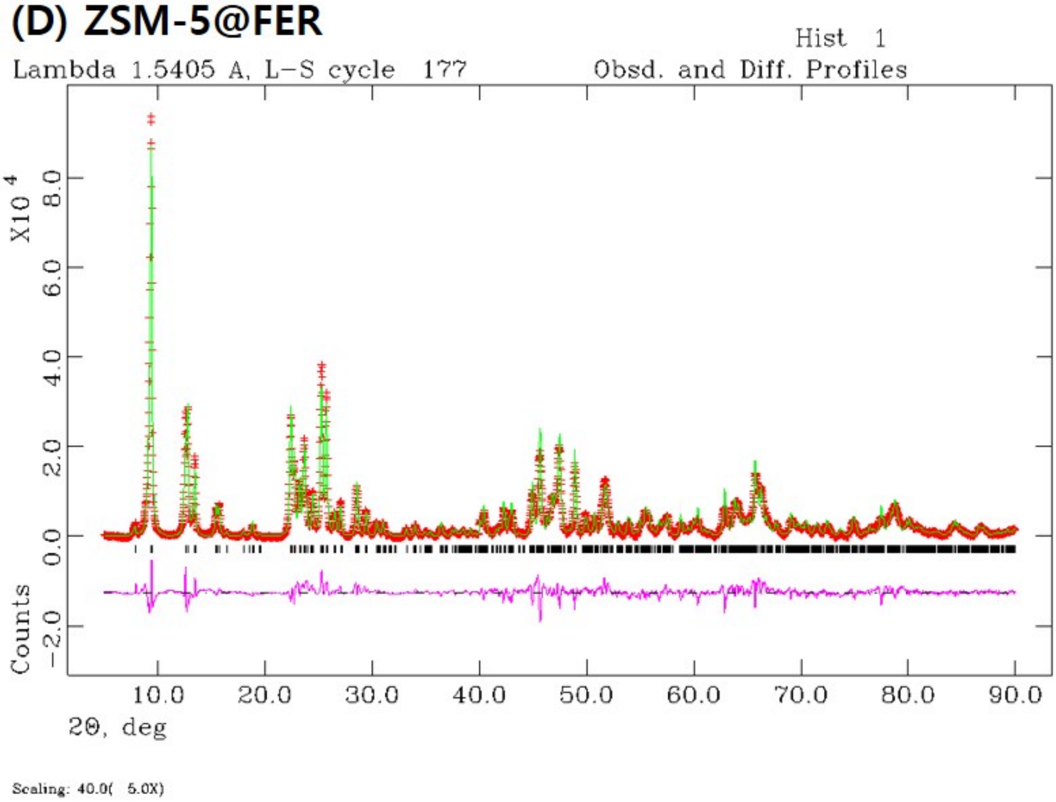

Figure S8. Rietveld refinement plot of four different seed-derived FER zeolites such as (A) FER, (B) FER@FER, (C) MOR@FER, (D) ZSM-5@FER and (E) USY@FER (continued)

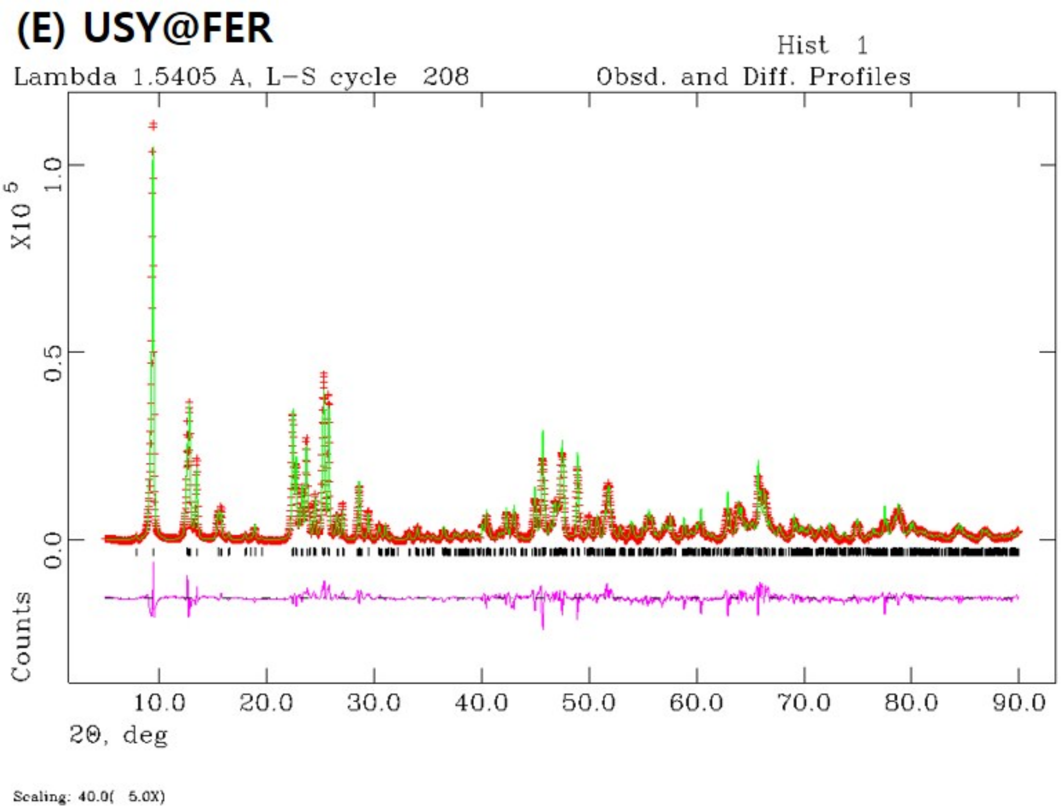

Figure S8. Rietveld refinement plot of four different seed-derived FER zeolites such as (A) FER, (B) FER@FER, (C) MOR@FER, (D) ZSM-5@FER and (E) USY@FER (continued)

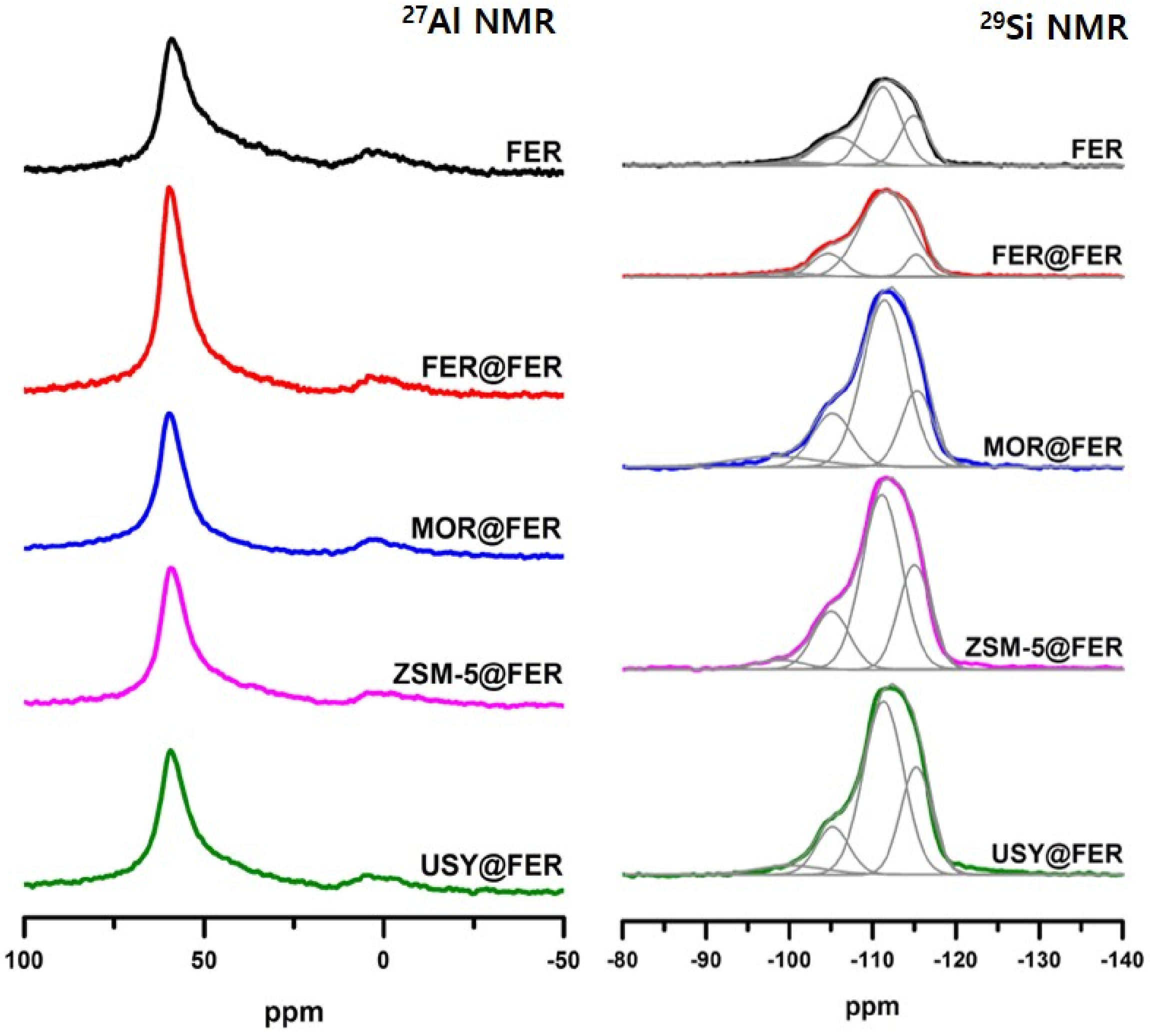

Notation	Si deconvolution (%) and chemical shift of ^{29}Si (ppm)				
	Si(2Al)	Si(1Al)	Si(0Al)	Si(0Al)	Sum (Si(0Al))
	-99	-105	-111	-115	(- 111 ~ - 115)
FER	4	22	55	25	80
FER@FER	5	12	75	7	82
MOR@FER	7	17	57	19	76
ZSM-5@FER	4	16	54	26	80
USY@FER	4	13	56	27	83

Figure S9. NMR spectra of the fresh seed-derived FER zeolites with ^{27}Al MAS NMR spectra, ^{29}Si MAS NMR spectra and deconvoluted area (%) of Al-O-Si structures

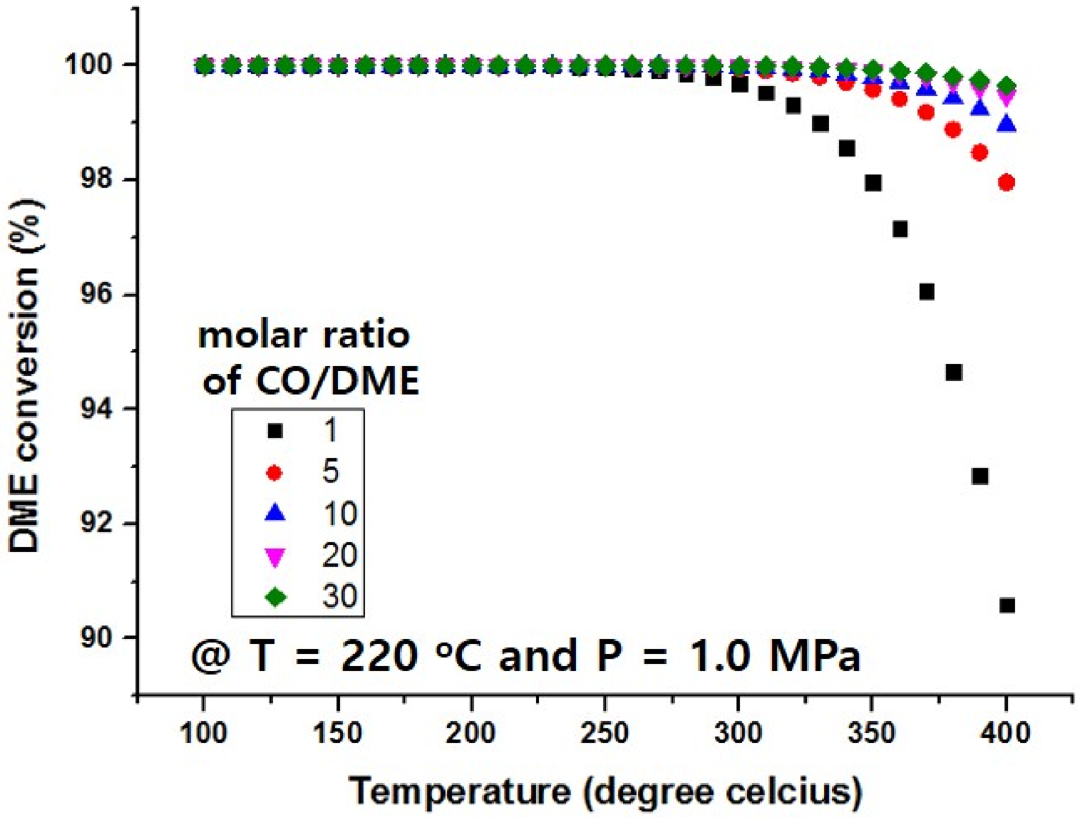

Figure S10. Equilibrium conversions of DME carbonylation to methyl acetate at the fixed pressure of 1.0 MPa with respect to reaction temperatures (100 – 400 °C) and CO/DME molar ratios (1 – 30)

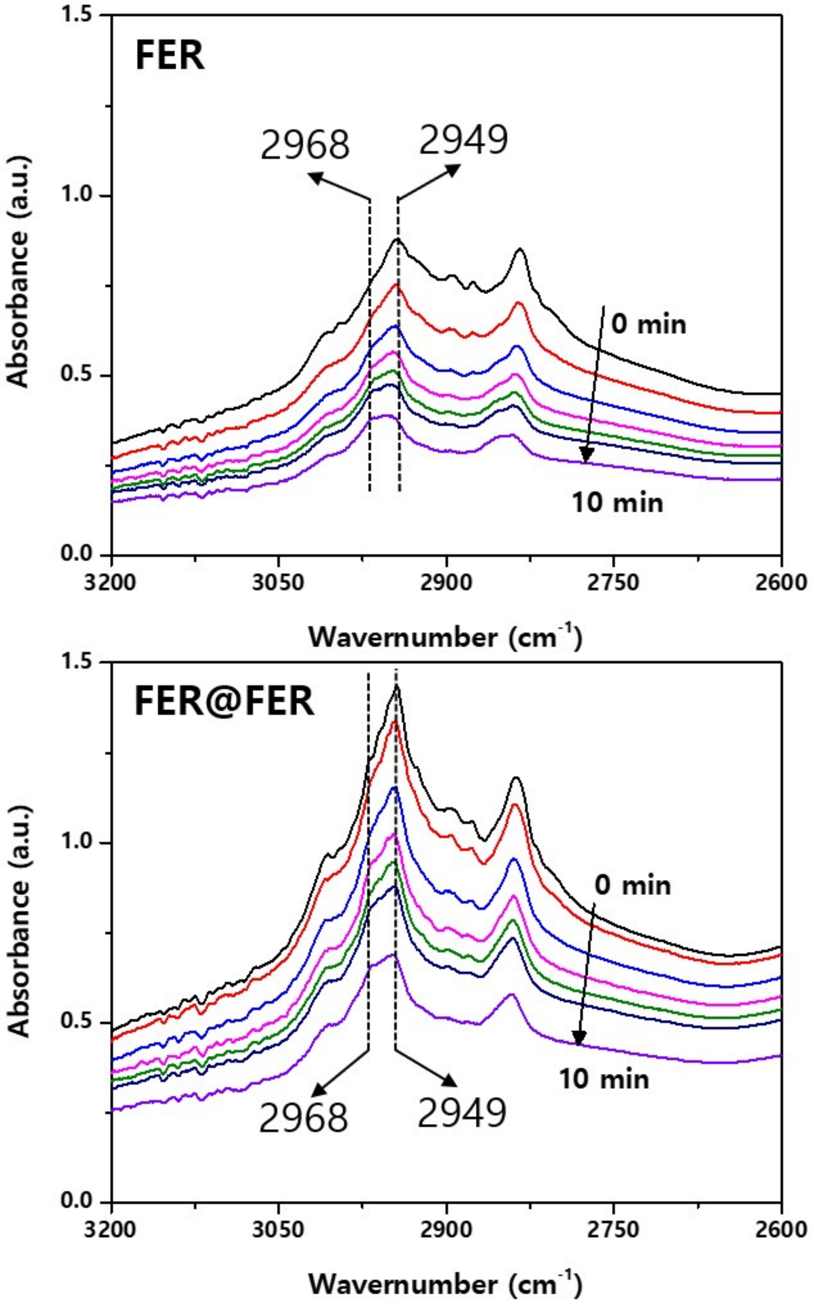

Figure S11. Variations of FT-IR spectra of the adsorbed methyl intermediates appeared at the bands of 2968 and 2949 cm^{-1} on the fresh FER and FER@FER through a successive adsorption experiment of DME followed by CO reactant at a fixed temperature of 220 ^{o}C

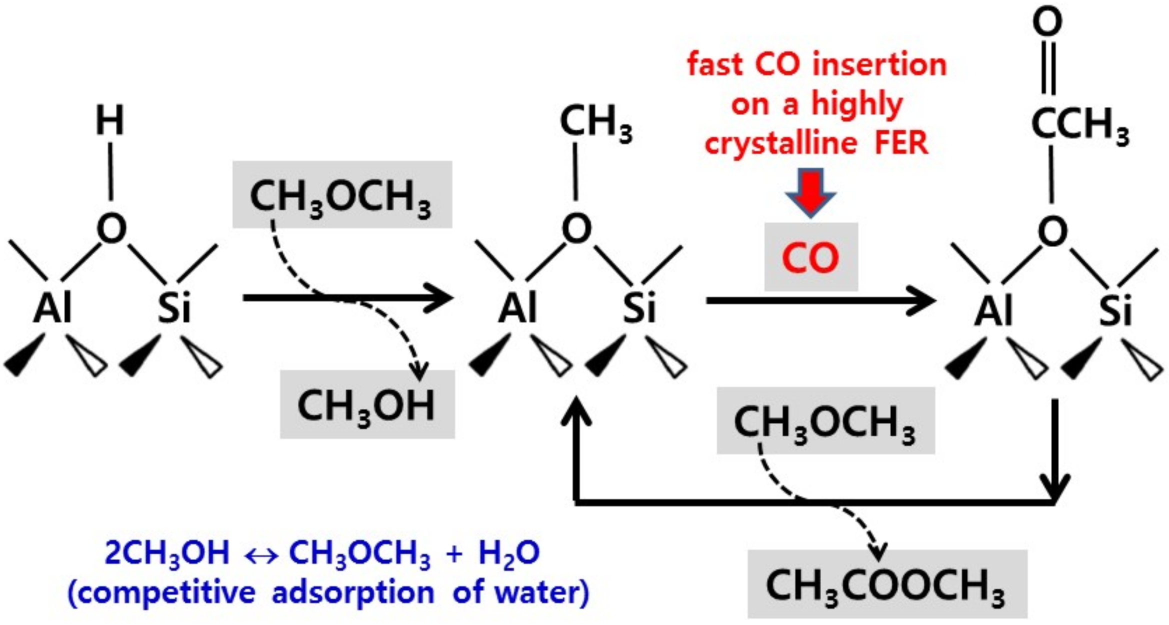

Scheme S1. Proposed reaction mechanisms on the highly crystalline FER@FER